Approach to the Parametric Design of Ion Thrusters

Paul J. Wilbur*
Colorado State University, Fort Collins, Colorado 80523
and
John R. Beattie† and J. Hyman‡
Hughes Research Laboratories, Malibu, California 90265

A methodology that can be used to evaluate ion thruster performance capabilities is presented. It can be applied to determine which of several physical constraints limit ion thruster power and thrust under various design and operating conditons. Results are presented for a typical case in which power and thrust are limited by grid system span-to-gap, intragrid electric field, discharge chamber power per unit beam area, and screen and accelerator grid lifetime constraints. In this case the thruster operating condition is selected to assure maximum thrust-to-power over a range of beam areas and specific impluses. It is pointed out that other operational objectives such as optimization of payload fraction or thrust duration for a mission of interest can be substituted readily for the thrust-to-power objective. An important result illustrated by an example case is that the specific impulse at which a typical ion thruster operates can be increased substantially above the value that produces maximum payload fraction without inducing a substantial loss in the payload fraction.

Nomenclature

A = area, m^2
B_0 = discharge chamber factor [see Eq. (16)]
d = diameter, m
E = allowable intragrid electric field, V/m
e = electron charge, C
F = thrust, N
$\tilde{F}_t$ = ion divergence thrust factor
f = fraction of ions produced
$\tilde{f}$ = ion focusing factor
g_{eo} = Earth surface gravitational acceleration, m/s^2
I_{sp} = specific impluse, s
J = current, A
j = current density, A/m^2
ℓ = length, m
M = molecular weight, kg/kgmole
m = mass, kg
$\dot{m}$ = mass flow rate, kg/s
N = allowable span-to-gap ratio
N_A = Avagadro's number
P = power, W
$\tilde{P}$ = primary electron rate factor, m^3/s
$\tilde{Q}$ = Maxwellian electron rate factor, m^3/s
S = sputtering yield
R = net-to-total accelerating voltage ratio
t = thickness
U = ion exhaust velocity, m/s
V = voltage, V
$\mathcal{V}$ = volume, m^3
v = velocity, m/s
α = multiply charged ion thrust correction factor
ϵ = energy cost, eV/ion
$\tilde{\epsilon}_0$ = permittivity of free space, f/m
γ = allowable erosion fraction
η = efficiency
ϕ = transparency
ρ = density, kg/m^3
ψ = enhancement factor
σ = inelastic collision cross section, m^2
τ = lifetime, s
F = beam flatness parameter

Subscripts
a = accelerator grid
B = beam
b = Bohm criterion
C = cathode or cathode potential surface
ce = charge exchange
D = discharge
e = effective
el = electrical
g = grids
M = Maxwellian electron
max = maximum
P = plasma
p = primary electron
s = screen grid
T = total
u = utilization of propellant
$+$ = singly charged
$++$ = doubly charged

Superscripts
$*$ = baseline value
$+$ = singly charged
$++$ = doubly charged
$'$ = primary electron

Introduction

ION thrusters are very attractive propulsion devices not only because of their high efficiency and high specific impluse capabilities but also because they afford potential users a great deal of operational flexibility. It is generally recognized, however, that providing the capability of changing operating conditions during a mission carries with it the price of a greater system complexity that cannot be justified for many missions. Selection of a single preferred design is therefore important, and it would be facilitated by the development of a methodology for evaluating and comparing vari-

Received Nov. 14, 1988; revision received June 30, 1989.

*Professor, Department of Mechanical Engineering. Member AIAA.
†Head, Plasma Sources Section, Ion Physics Department. Member AIAA.
‡Manager, Ion Physics Department. Member AIAA.

ous thruster options. Such a methodology would also help identify the research areas most likely to yield thruster performance gains.

An empirical methodology designed to accomplish these goals has been described by Byers and Rawlin[1] and Byers.[2] The approach used here is different from the one they used; it is based on relatively straightforward physical models that describe ion thruster phenomena rather than empirical relationships. Where nonideal behavior must be described, every attempt is made to do so by using parameters that are physically meaningful and commonly used. The objective of this paper is, then, to present a methodology that can be used to determine which of many possible performance-constraining phenomena, characterized by thruster design and operational parameters, will be limiting for a specified mission or class of missions. A second objective is to illustrate how information on this subject might be presented in a format that is easy to understand.

Theory

The principal ion thruster design variables are specific impulse I_{sp}, beam are a A_B, and beam power P_B. Generally, one would want to select the specific impulse and beam area of a device and then determine the beam power at which it should be operated. In this development specific impulse and beam area will, therefore, be treated as independent variables, and beam power will be treated as the dependent variable.

Examples of physical constraints that have been found to limit the beam power at which a thruster can operate include the following.

1) *Grid system span-to-gap ratio.* This constraint is determined by the extent to which grids can be held uniformly close together in an environment of thermally induced distortion and in some situations significant electrostatic attraction. It is influenced greatly by mechanical design and fabrication considerations. A value of 600 might be considered a reasonable limit for conventional circular grids,[3] but future, nonconventional designs could facilitate substantial increases above 600.

2) *Intragrid electric field.* An excessively high electric field between the screen and accelerator grids of a thruster results in electrical breakdown, which precludes ion beam extraction. This limit is influenced by such factors as the surface finish and uniformity of intragrid spacing. Typical values in operating thrusters have generally been about 2 kV/mm, although higher values have been reported in laboratory tests.[4]

3) *Discharge power per unit beam area.* This constraint reflects a heat transfer limit that develops because components such as magnets, anodes, or grids can overheat if the heat transferred to them via the discharge plasma becomes too great. This constraint could be formulated in terms of specific heat transfer limitations for particular components and radiative boundary conditions between adjacent components and thrusters. For the illustrative purposes of this paper, however, it will be assumed that the allowable discharge power scales directly with beam area and that a limit in the range of 15–20 kW/m^2 is reasonable.

4) *Screen grid lifetime.* The lifetime of the screen grid and other components exposed to the discharge plasma is limited by the process of ion-induced sputter erosion. Typically, design lifetimes in the range of 10^4 to 2×10^4 h are sought, and they are influenced by the discharge voltage and the materials and ions involved.

5) *Accelerator grid lifetime.* The accelerator grid is exposed to small currents of high energy, charge-exchange ions that limit its lifetime. It would generally be designed to have a lifetime in the same 10^4 to 2×10^4 h range as the screen grid.

The above list of constraints on ion thruster design is not exhaustive, but these particular ones have been observed in various thrusters, and they can be used for purposes of illustration. Further, radical new designs could introduce dramatic changes in the values used or even supersession of some constraints.

A tradeoff exists between the mass requirements for ion thruster propellant and power, and, for this reason, preferred operating points, which can be defined *by operational objectives*, exist. The objective selected influences the severity of each design constraint thereby determining the power limitation imposed by it. Typical operational objectives might stipulate thruster operation at maximum thrust per unit input power or maximum payload fraction on a prescribed mission. They might also be expressed in a complex algorithm that has been incorporated into a mission analysis routine and optimizes some other mission objective.

Mathematical Development

The beam power P_B produced by an ion thruster is expressed most simply as the product of beam current J_B and beam (or net accelerating) voltage V_B.

$$P_B = J_B V_B \tag{1}$$

The beam current in this equation is related to the peak current density being extracted through the grids $j_{B\max}$ and the beam area A_B through the beam flatness parameter F, which is defined as the ratio of average-to-peak ion beam current densities.

$$F = J_B/(j_{B\max}A_B) \tag{2}$$

It is noted that the flatness parameter can be calculated for a particular thruster design using the finite element technique developed by Arakawa and Wilbur.[5] For purposes of illustration here, it will be assigned a reasonable, constant value (0.5).

The maximum current density capability of a grid set is determined by space-charge limitations, which may be quantified approximately using the one-dimensionally based Child-Langmuir law.[6]

$$j_{B\max} = \frac{4\tilde{\epsilon}_0}{9}\left(\frac{2e}{m_i}\right)^{1/2}\frac{V_T{}^{3/2}}{\ell_e^2}\phi_s\psi_e \tag{3}$$

The permittivity of free space $\tilde{\epsilon}_0$, the electron charge e, and the ion mass m_i are known constants, and the total accelerating voltage V_T and the screen grid transparency to ions ϕ_s are at the control of the designer. The ion current density enhancement factor ψ_e accounts for increased current density capabilities that can be induced by ions that approach the screen grid plasma sheath at nonzero velocities[6] or high-energy electrons injected into the sheath[7] to mitigate the space-charge effect. It will be assigned a value of unity for this study. The effective ion acceleration length ℓ_e in Eq. (3) is determined by span-to-gap and electric-field constraints that remain to be expressed mathematically at this point in the development. It is noted, however, that the value of ℓ_e is assumed here to be the same for each of the aperture pairs in the grids.

The total accelerating voltage that appears in Eq. (3) can be eliminated in favor of the beam voltage by introducing the net-to-total accelerating voltage ratio R

$$R = V_B/V_T \tag{4}$$

The beam voltage can now be related to the specific impulse I_{sp} by recognizing that the specific impulse is defined as the thrust F per unit weight flow rate of propellant $\dot{m}g_{eo}$

$$I_{sp} = F/\dot{m}g_{eo} \tag{5}$$

that the thrust is given by

$$F = [\dot{m}\eta_u]\ [U\tilde{F}_t\alpha] \tag{6}$$

and that the ion exhaust velocity U is related to the beam voltage through the conservation of energy expression

$$V_B e = m_i U^2/2 \tag{7}$$

In Eq. (6) the product of propellant mass flow rate $\dot{m}$ and propellant utilization efficiency η_u, which is the first bracketed term, represents the flow rate of thrust producing (high velocity) propellant. The second bracketed term in Eq. (6) represents the effective jet velocity of the beam ions. This term includes two efficiency factors, one ($\tilde{F}_t$) that reflects that many ions will emerge from the grid system on divergent trajectories.[8] The other factor α accounts from the fact that the velocity of singly charged ions [from Eq. (7)] is used in Eq. (6), but some multiply charged ions will generally be produced and extracted, and their effect must be reflected properly.

Combining Eqs. (5-7), the desired expression for beam voltage in terms of specific impulse is obtained

$$V_B = \frac{m_i}{2e}\left(\frac{I_{sp}\, g_{eo}}{\eta_u \tilde{F}_t \alpha}\right)^2 \tag{8}$$

and this may be combined with Eqs. (1-4) to obtain

$$P_B = \frac{\tilde{\epsilon}_0 F A_B \phi_s \psi_e}{9\ell_e^2 R^{3/2}} \left(\frac{m_i}{e}\right)^2 \left(\frac{I_{sp}\, g_{eo}}{\eta_u \tilde{F}_t \alpha}\right)^5 \tag{9}$$

Equation (9) defines the maximum power constraint associated with the ion extraction process as a function of the thruster beam area and specific impulse. Two physical constraints (allowable span-to-gap and intragrid electric field) are imposed through the effective ion acceleration length ℓ_e. The fact that propellant utilization appears in the equation serves as a reminder that an operational objective must also be defined before unique limiting values of beam power can be computed as a function of specific impulse and beam area for these physical constraints.

Span-to-Gap Constraint

The allowable span-to-gap ratio N associated with traditional grid sets is the grid diameter-to-spacing ratio. In order to accommodate noncircular beam cross sections; however, this ratio will be defined here using an equivalent beam diameter, and the grid separation will be given by the expression

$$\ell_g = \frac{\sqrt{4\, A_B/\pi}}{N} \tag{10}$$

The ion acceleration length appearing in Eq. (9) is based on one-dimensional theory. The ion acceleration process that occurs in an ion thruster, however, is two dimensional, and ℓ_e should be selected so it will yield the correct beam current density associated with this two dimensionality. One value of ℓ_e that should come close to doing this is illustrated in Fig. 1. It is related to the grid separation distance given by Eq. (10) through the expression

$$\ell_e = \sqrt{(t_s + \ell_g)^2 + d_s^2/4} \tag{11}$$

It is noted here that Eq. (11) differs from the traditional equation for ℓ_e used to compute perveances[9] in that it accounts for the screen grid thickness t_s. If the screen grid thickness is left out of this expression, the implication is that the screen hole sheath positons itself close to the downstream edge of the screen grid. Aston and Wilbur[10] have shown, however, that this sheath is located near the upstream edge of the hole under normal operating conditions, and Eq. (11) is therefore considered correct.

Equations (9-11) can be combined to define the maximum beam power at which a thruster with a beam area A_B and a span-to-gap ratio N can be operated. This can be done as a function of specific impulse, provided an operational objective, a screen grid thickness t_s, and a screen hole diameter d_s are specified. For this illustrative study, these latter two parameters have been defined by specifying a grid separation-to-screen hole diameter ratio ℓ_g/d_s and screen grid thickness of unity and 0.0005 m, respectively.

Electric Field Constraint

In order to prevent electrical breakdown between grids, it is presumed that a limiting electric field E cannot be exceeded. Assuming a uniform grid spacing, this may be expressed mathematically as

$$\ell_g = \frac{V_T}{E} = \frac{V_B}{R\,E} \tag{12}$$

Combining this with Eqs. (9) and (11), an operational objective, a screen-grid thickness, and a screen-grid hole diameter, the beam power/beam area/specific impulse surface limited by electrical breakdown considerations is defined.

Discharge Chamber Thermal Constraint

If the ion thruster discharge chamber power is too great, failures related to magnet, screen grid, or anode overheating could occur. Of course the allowable discharge power should scale with thruster size. A review of limiting discharge powers on thrusters having various diameters has suggested that it is probably the discharge power per unit beam area P_D/A_B that defines this constraint. It is suggested that a value of 15-20 kW/m^2 might be a reasonable limit for typical thrusters that have been built.

The discharge power can be expressed in terms of the energy cost of a beam ion ϵ_B through the equation

$$\frac{P_D}{A_B} = \frac{\epsilon_B J_B}{A_B} \tag{13}$$

Combining Eqs. (1), (8), and (13), one obtains

$$P_B = \left(\frac{P_D}{A_B}\right)\left(\frac{A_B}{\epsilon_B}\right)\left(\frac{m_i}{2e}\right)\left[\frac{I_{sp}\, g_{eo}}{\eta_u \tilde{F}_t \alpha}\right] \tag{14}$$

The beam ion energy cost appearing in this equation can be computed using Brophys model[11] in the form

$$\epsilon_B = \frac{\epsilon_p^*}{f_B}\left[\left\{1 - \exp\left[-B_0(1-\eta_u)\right]\right\}\right]^{-1} + \frac{f_C V_D}{f_B} \tag{15}$$

when the propellant and discharge voltage V_D are prescribed so that the baseline plasma ion energy cost ϵ_p^* can be determined.[11] The fractions of ions produced that go to cathode potential surfaces f_C and into the beam f_B are determined by

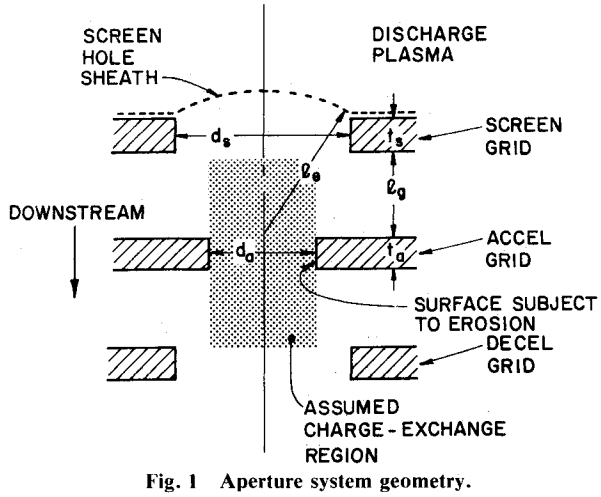

Fig. 1 Aperture system geometry.

the chamber and magnetic field geometry.[11,5] The parameter B_0 is given by

$$B_0 = \dot{m}C_0 = \frac{4\,\sigma'0\,\ell^*}{m_i\,v_0\,\phi_0}\left(\frac{\dot{m}}{A_B}\right) \tag{16}$$

where C_0 is the primary electron utilization factor, σ_0' the primary electron/propellant atom total inelastic collision cross section, and the propellant atom thermal velocity v_0 may be assumed constant for a particular propellant and discharge voltage. The transparency of the grids to neutral atoms ϕ_0 and the primary electron containment length ℓ^* can be calculated and estimated using, respectively, an equation and typical experimental results given by Brophy.[11] An expression for the propellant flow rate per unit beam area needed in Eq. (16) can be obtained by combining the definition of propellant utilization efficiency

$$\eta_u = \frac{J_B m_i}{\dot{m}e} \tag{17}$$

with Eqs. (2-4) and (8) to obtain

$$\frac{m}{A_B} = \frac{2\,\tilde{\epsilon}_0\,F\,\phi_s\psi_e}{9\,\eta_u^4\,\ell_e^2\,R^{3/2}}\left(\frac{m_i}{e}\right)^2\left[\frac{I_{sp}\,g_{eo}}{\tilde{F}_t\alpha}\right]^3 \tag{18}$$

Equations (14-16), and (18), when combined with an operational objective, yield the beam power/beam area/specific impulse surface that defines the discharge power per unit beam area constraint.

Screen Grid Lifetime Constraint

Althought the screen grid is assumed to be the life limiting component subjected to sputter erosion in this paper, other components that are subjected to plasma ion bombardment could impose additional similar constraints. They could be incorporated into the analysis using equations similar to those developed here for the screen grid. If the screen grid lifetime is considered to have expired when a fraction γ_s of its initial thickness t_s has been sputtered away, then this lifetime will be given by[8]

$$\tau_s = \frac{e\rho_s N_A\,\gamma_s\,T_s}{M_s[j_{P+}S_s^+(V_D) + 0.5\,j_{P++}S_s^{++}(2V_D)]} \tag{19}$$

The sputtering yields of the grid material for singly and doubly charged ions [$S_+(V_D)$ and $S_{++}(2V_D)$] are evaluated respectivley for ions with energies equal to the discharge voltage and twice the discharge voltage as the symbolism suggests. Recognizing that the grid will sputter most rapidly at the point of maximum current density ($j_{P+} \approx j_{B\max}$), Eqs. (1), (2), and (8) can be combined with Eq. (19) to obtain

$$P_B = \frac{m_i\,\rho_s\,N_A\,\gamma_s t_s\,FA_B}{2\tau_s M_s\left[S_s^+(V_D) + 0.5\,\frac{j_{P++}}{j_{P+}}S_s^{++}(2V_D)\right]} \times \left(\frac{I_{sp}\,g_{eo}}{\tilde{F}_t\alpha}\right)^2 \tag{20}$$

The doubly-to-singly charged discharge plasma ion current density ratio j_{P++}/j_{P+} appearing in this equation is a strong function of discharge operating conditions and is given by[11]

$$\frac{j_{P++}}{j_{P+}} = \frac{2\left(\tilde{Q}_+^{++}\frac{n_p}{n_M}\tilde{P}_0^{++}\right)}{\tilde{Q}_0^+ + \frac{n_p}{n_M}\tilde{P}_0^+} + 0.83\left(\frac{v_0}{v_b}\right)\left(\frac{\phi_0}{\phi_s}\right) \times \left[\frac{\tilde{Q}_+^{++}\frac{n_p}{n_M}\tilde{P}_+^{++}}{\tilde{Q}_0^+ + \frac{n_p}{n_M}\tilde{P}_0^+}\right]\frac{\eta_u}{1-\eta_u} \tag{21}$$

Some simplification of this equation is generally possible because the first term is negligible at typical discharge chamber electron temperatures and energies. In Eq. (21), the Bohm[12] and neutral atom thermal velocities v_b and v_0 are evaluated based on the electron and discharge chamber wall temperatures, respectively. The rate factors associated with production of the various ionic species $\tilde{Q}_0^+$, $\tilde{P}_0^+$, etc., are determined by the prevailing discharge plasma electron temperatures and energies.[13] The primary-to-Maxwellian electron density ratio n_p/n_M appearing in Eq. (21) is given by[11]

$$\frac{n_p}{n_M} = \left\{\left[\left(\frac{0.15\,e\epsilon_p^* v_b\phi_0\phi_s}{v_p V_D f_B\sigma_0'}\right)\left(\frac{A_B}{\dot{m}}\right)\left(\frac{A_B}{\forall_p}\right) \times \frac{1}{1-\eta_u}\right]^{-1} - 1\right\}^{-1} \tag{22}$$

In this equation, the primary electron velocity v_p is determined by the primary electron energy, which is assumed to be equal to the discharge voltage. The discharge chamber plasma volume-to-beam area ratio $\forall_p/A_B$ is approximately the discharge chamber length, which may be assumed to be relatively insensitive to beam area.

The final expression needed to define the screen grid lifetime constraint is one for the propellant mass flow rate per unit beam area. It is obtained by combining Eqs. (1), (8), and 17.

$$\frac{\dot{m}}{A_B} = \frac{2P_B\,\eta_u}{A_B}\left[\frac{\tilde{F}_t\,d}{I_{sp}\,g_{eo}}\right]^2 \tag{23}$$

Equations (20-23) can be solved for the beam power/beam area/specific impulse surface that defines the screen-grid lifetime constraint when an operational constraint, grid thickness, propellant, and discharge voltage have been specified.

Accelerator Grid Lifetime Constraint

For a three-grid ion optics system where sputtering on the barrel (interior surface) region of the accelerator grid holes determines the accel grid lifetime, the change in accelerator hole diameter d_a per unit time for the hole subject ot the most rapid erosion is given by

$$\frac{d(d_a)}{d\tau_a} = \frac{S_a\,j_{B\max}n_0\sigma_{ce}\forall_{ce}\tilde{f}_a M_a}{eN_A\rho_a\pi d_a t_a} \tag{24}$$

The sputter yield of the accelerator grid material S_a is evaluated at the prevailing charge-exchange ion kinetic energy, and the neutral atom density in the charge exchange reaction region n_0 should reflect contributions from both thruster propellant flow and background gases. The volume of the charge exchange region $\forall_{ce}$ and the factor describing the extent to which these ions are focused onto the barrels of the accel apertures $\tilde{f}_a$ are both probably dependent on a number of factors. The dependencies are, however, not well understood. For a two-grid optics set, where sputtering occurs on the downstream surface of the accelerator grid, a similar equation[8] is used, but for the example study being done here, the three-grid equation [Eq. (24)] will be used exclusively.

For a thruster operating in a low background pressure environment, the neutral atom density in the charge exchange region is given approximately by the expression

$$n_0 = \frac{4J_B(1-\eta_u)}{A_B\,\phi_0 v_0 e} \tag{25}$$

If the allowable change in diameter is Δd_a, and τ_a is the desired lifetime, then an approximate form of Eq. (24) may be combined with Eqs. (1), (2), (8), and (25) to obtain

$$P_B \approx \frac{A_B m_i}{4}\left[\frac{F\phi_0 v_0 N_A \rho_a t_a(\Delta d_a/d_a)}{\tau_a S_a(1-\eta_u)\,\sigma_{ce}\tilde{f}_a M_a\,\ell_g}\right]^{1/2}\left[\frac{I_{sp}\,g_{eo}}{\eta_u\,\tilde{F}_t\alpha}\right] \quad (26)$$

In order to compute beam power as a function of beam area and specific impulse using this equation, the volume of the charge exchange region has been assumed to be a cylinder with a diameter equal to that of the accelerator grid aperture d_a and length twice the grid separation distance ℓ_g. In addition, the ratio of accelerator grid thickness to grid separation distance t_a/ℓ_g has been assumed to be constant.

Operational Objective

An operational objective must be specified to define the thruster discharge chamber operating point, i.e., the propellant utilization efficiency or discharge power at which the thruster should be operated. This can be done, for example, by defining a mission of interest and then selecting the propellant utilization efficiency to maximize the payload fraction. In such a case, the mission could be characterized very simply by a mission time and characteristic velocity or in terms of a complex mission algorithm. The optimum propellant utilization operating point might also be selected to ensure thruster operation at maximum thrust to power.[14] For the sample analysis being presented here, this latter operational objective is applied. The objective is developed from the following expression for thruster electrical efficiency:

$$\eta_{el} = \frac{P_B}{P_T} = \frac{J_B\,V_B}{J_B\,V_B + \Sigma P} \quad (27)$$

In this equation ΣP is the sum of the powers needed to produce ions and sustain thruster temperatures, propellant flow rates, and neutralizer operation. Frequently, this term is dominated by the discharge power required to produce the ions and it can be expressed in terms of the energy cost of a beam ion (i.e., as $P_D = J_B \epsilon_B$).

Assuming the discharge power does dominate the losses, Eq. (27) can be rewritten as

$$\eta_{el} = \frac{V_B}{V_B + \epsilon_B} \quad (28)$$

This equation can be combined with Eqs. (5–8), (17), and (18) to obtain the expression for thrust-to-total power.[14]

$$\frac{F}{P_T} = \frac{I_{sp}\,g_{eo}}{\eta_u}\left[\frac{1}{\frac{1}{2}\left(\frac{I_{sp}\,g_{eo}}{\eta_u\,\tilde{F}_t\alpha}\right)^2 + \frac{\epsilon_B e}{m_i}}\right] \quad (29)$$

By seeking the propellant utilization that maximizes this equation at each specific impulse, operation at maximum thrust to power can be assured at each thruster beam area and physical constraint condition.

Results

The analysis technique outlined in the preceding section can be used to investigate the effects of a wide variety of design and operational parameters on the power and thrust capabilities of ion thrusters. The purpose of this paper is to demonstrate the capability of the methodology involved rather than to draw conclusions based on an exhaustive study conducted using it. Consequently, a single set of typical thruster parameters has been selected for use in analysis. The values used are listed in Table 1, and though they are considered to be typical of ion thrusters in general, they do not represent any particular thruster. The rate factors used in the analysis are based on an assumed Maxwellian electron temperature of 5 eV and a primary electron energy of 30 eV. The superscripts on the parameter names in this table designate references from which values were obtained.

If one prescribes a beam area, the beam power limits for each of the physical constraints described in the preceding section can be determined for a thruster operating at maximum thrust to power. Figure 2 shows the limits imposed when the constraints take on the values indicated, and the thruster beam area is 0.2 m^2. Operation below and to the right of each curve assures operation that does not violate the associated constraint. Hence, in the case of Fig. 2, the 600 span-to-gap constraint limits the power that can be extracted up to a specific impulse of ~3000 s and then the 2-kV/mm electric field constraint becomes limiting. For the particular parameters associated with the other constraints, Fig. 2 indicates that

Table 1 Thruster parameters used in example study in the order of their appearance

Parameter	Symbol	Value used
Ion beam flatness	F	0.5
Ion current density enhancement factor	ψ_e	1.0
Screen grid transparency to ions	ϕ_s	0.7
Grid system transparency to neutral atoms	ϕ_0	0.16
Ion mass (xenon)	m_i	2.2×10^{-25} kg
Net-to-total accelerating voltage ratio	R	0.5
Beamlet divergence thrust factor	$\tilde{F}_t$	1.0
Multiply charged ion thrust factor	α	1.0
Screen grid thickness	t_s	5×10^{-4} m
Grid separation to screen hole diameter ratio	ℓ_g/d_s	1.0
Baseline plasma ion energy cost	ϵ_p^*	50 eV/ion
Extracted ion fraction	f_B	0.5
Fraction of plasma ions going to cathode potential surfaces	f_C	0.3
Discharge voltage	V_D	30 V
Primary electron-atom inelastic collision cross section[15,16]	$\sigma\acute{o}$	7.4×10^{-20} m^2
Primary electron containment length	ℓ^*	3.5 m
Neutral atom thermal velocity	v_0	290 m/s
Allowable screen grid erosion fraction	γ_s	0.5
Ionization rate factors for 5-eV temperature Maxwellian electrons[13]	$\tilde{Q}_0^+$	7.1×10^{-15} m^3/s
	$\tilde{Q}_+^{++}$	5.1×10^{-16} m^3/s
Ionization rate factors for 30-eV energy primary electrons[13]	$\tilde{P}_0^{++}$	1.3×10^{-13} m^3/s
	$\tilde{P}_+^{++}$	2.5×10^{-14}m^3/s
Sputter yields for molybdenum screen grid hit by singly and doubly charged xenon ions[17]	S_s^+	2×10^{-6}
	S_s^{++}	1.5×10^{-3}
Sputter yield for accelerator grid[17]	S_a	1.0
Charge exchange cross section[18]	σ_{ce}	3×10^{-19}m^2
Accelerator grid thickness-to-grid separation ratio	t_a/ℓ_g	0.3
Allowable accelerator grid erosion	$\Delta d_a/d_a$	0.5
Charge exchange ion focusing factor	$\tilde{f}_a$	1.0

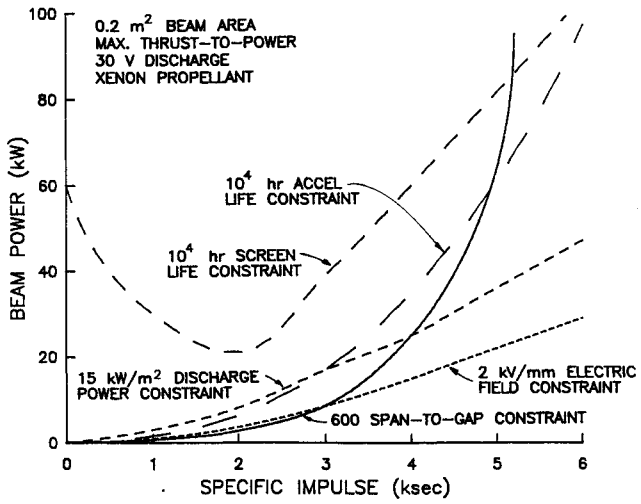

Fig. 2 Typical power constraint curves, 0.2-m² beam area (span-to-gap and intragrid electric field limiting).

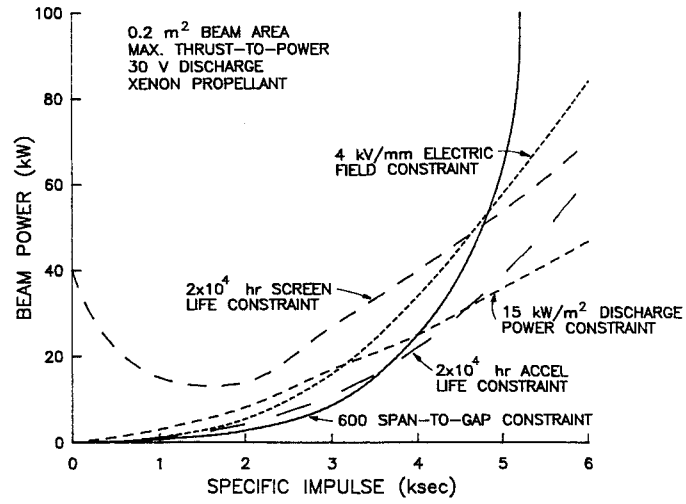

Fig. 4 Typical power constraint curves, 0.2-m² beam area (span-to-gap, discharge power, and accelerator grid lifetime limiting).

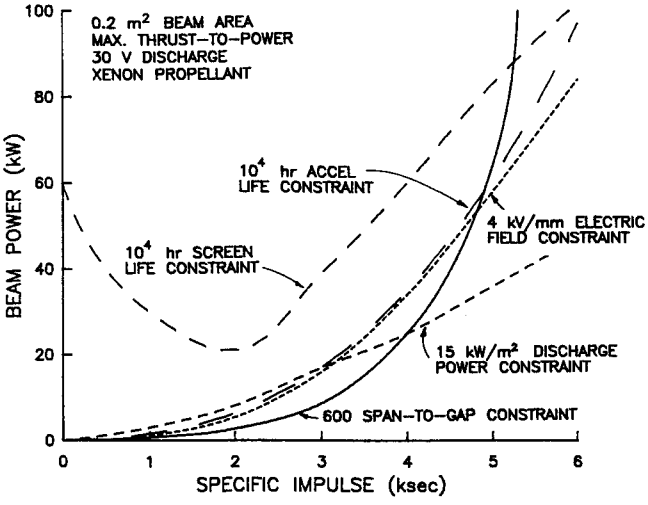

Fig. 3 Typical power constraint curves, 0.2-m² beam area (span-to-gap and discharge power limiting).

none of the other constraints (discharge power, screen grid life, or accelerator grid life) become limiting at any specific impulse up to 6000 s.

If the grids were designed so that the electric field limit could be increased to 4 kV/mm, and the other constraints were held fixed at the values of Fig. 2, the data of Fig. 3 are generated. They suggest the 600 span-to-gap limit would prevail to ~4000 s specific impulse, and the discharge power per unit beam area limit of 15 kW/m² would become constraining beyond that point. Increasing the electric field limit in this case allows the beam power at 4000-s specific impulse to increase from ~15 kW (Fig. 2) to ~25 kW (Fig. 3) and from ~27 kW (Fig. 2) to 45 kW (Fig. 3) at 6000 s. If, on the other hand, it was necessary to have screen and accelerator grid lifetimes of 2×10^4 h, then the accelerator grid lifetime would become limiting over the specific impulse range from about 3500–4500 s as the data of Fig. 4 show. In this case, the power at 4000-s specific impulse would be limited by accelerator grid lifetime considerations to ~21 kW.

If the beam power limits imposed by the constraints are sought as functions of both beam area and specific impulse rather than holding beam area constant, then equal beam power contour plots like the ones shown in Fig. 5 can be generated. The contours shown define power limits constrained by the physical limit indicated on each plot; operation below the power indicated on any contour is allowed. When all constraints are imposed simultaneously, a global contour map like the one shown in Fig. 6 is obtained. As the labels on the two regions of this contour map indicate, the span-to-gap and electric-field constraints are most restrictive. Span to gap limits beam power at low specific impulses and electric field limits it at higher ones over the beam area range from 0 to 1 m².

If one defines a mission along with power-processor specific mass parameters and then imposes the power limits defined by all of the constraints associated with the data in Fig. 5, payload fractions can be computed as a function of beam area and specific impulse. Figure 7 shows the payload fraction contour map computed when the most restrictive constraint is imposed at each beam area and specific impulse for a 10^4-m/s mission to be accomplished in 0.67 year when the powerplant and power conditioner are characterized by the specific masses and the power conditioner efficiency values cited in the figure title. The payload fraction is seen to reach a relatively flat peak at a value of 55% when the specific impulse is near 4500 s for all but the smallest beam areas. The payload fraction peak in Fig. 7 is seen to be very broad so that the thruster could be operated at any specific impulse in the range between ~3000–6000 s and it would deliver about the same payload fraction. This point is important because it indicates operation at an off-optimum specific impulse may be pursued to realize some other objective (e.g., simplified fabrication, greater reliability, or lower cost) without necessarily suffering a significant loss in payload fraction.

The thrust at which the ion thruster operates can also be computed as a function of beam area and specific impulse using Eq. (29). Figure 8 shows how the thrust is constrained as a function of beam area and specific impulse when the constraints pertaining to Figs. 5 and 6 are imposed.

If the electric field limit is increased from 2 to 4 kV/mm, the results of Fig. 3 show that the discharge power per unit beam area becomes power limiting at high specific impulses when the beam area is 0.2 m². The effect of introducing this same electric field limit for beam areas ranging from 0 to 1.0 m² is shown in Fig. 9. Comparison of the data in Figs. 6 and 9 shows that increasing the electric field limit causes the discharge power constraint to become limiting and facilitates a substantial increase in beam power at high specific impulses.

If the grid lifetime requirements are increased to 20,000 h while the 4-kV/mm electric field constraint is maintained, the results shown in Fig. 10 are obtained. In this case the 20,000 h accelerator grid lifetime constraint limits beam power in the intermediate specific impulse low beam area regime shown. Away from this region, the power limit is unchanged from the values presented in Fig. 9.

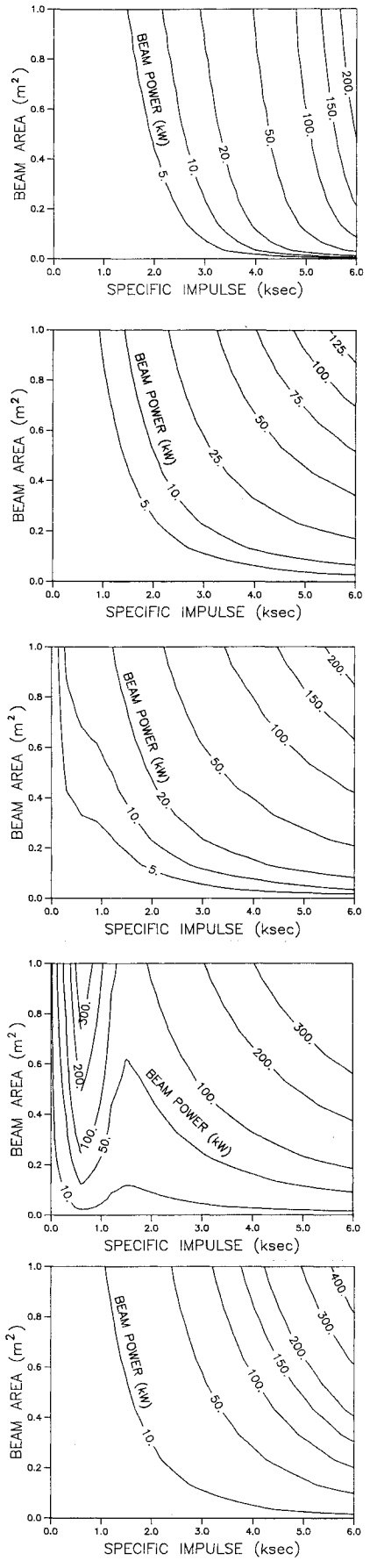

Fig. 5 Typical individual power constraint contour maps: a) span-to-gap limited to 600; b) intragrid electric field limited to 2 kV/mm; c) discharge power/beam area limited to 15 kW/m²; d) screen grid erosion lifetime limited to 10^4 hr.; e) accelerator grid erosion lifetime limited to 10^4 h.

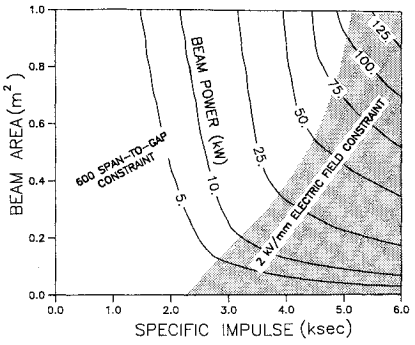

Fig. 6 Typical global power constraint contour map (600 span-to-gap and 2-kV/mm intragrid electric field limiting).

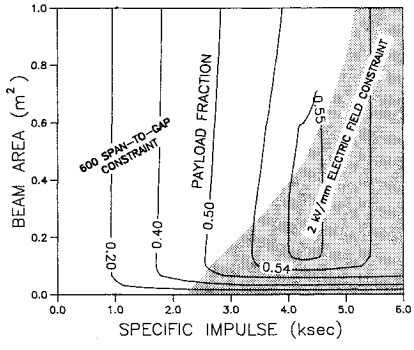

Fig. 7 Typical global payload fraction contour map (600 span-to-gap and 2-kV/mm intragrid electric field limiting).

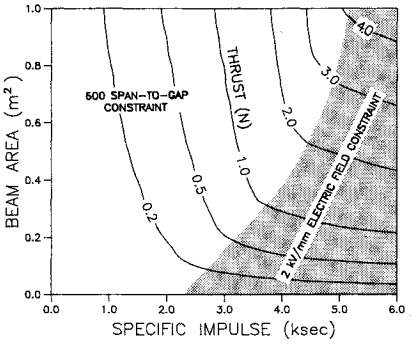

Fig. 8 Typical global thrust contour map (600 span-to-gap and 2-kV/mm intragrid electric field limiting), mission $\Delta V = 10^4$ m/s, mission time = 0.67 yr, powerplant specific mass = 15 kg/kW, power conditioner specific mass = 4.5 kg/kW, power conditioner efficiency = 95%.

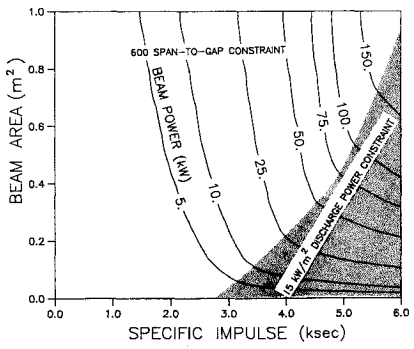

Fig. 9 Typical global power constraint contour map (2 kV/mm span-to-gap and 15 kW/m² discharge power limiting).

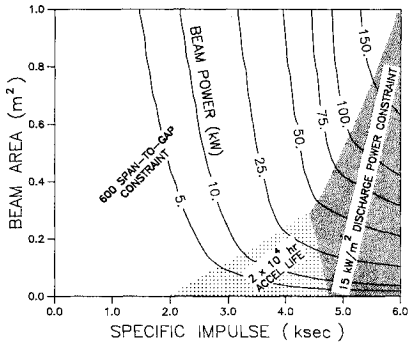

Fig. 10 Typical global power constraint contour map (600 span-to-gap and 15 kW/m^2 discharge power and 2×10^4 h accelerator grid life limiting).

Future Directions

The intent of this work has been to 1) present a methodology and framework within which gross parameters describing ion thruster behavior could be used to predict ion thruster performance limits, 2) cite references that describe how these gross parameters can be computed, and 3) suggest how results obtained from the analysis might be presented in a readily understood format. This analysis should, however, not be considered fully developed. The following are examples of changes that could be introduced to improve the analysis.

1) The beamlet divergence (thrust) factor $\tilde{F}_t$, the grid separation-to-screen hole diameter ratio ℓ_g/d_s, and the net-to-total acceleration voltage ratio R have all been treated as constants in the cases analyzed. These quantities are, however, variable and they are related to each other. Data like those in Ref. 19 could be used to determine values of $\tilde{F}_t$ for prescribed values of ℓ_g/d_s and R. A more ambitious step would be to allow ℓ_g/d_s and R and consequently $\tilde{F}_t$ to be varied along with propellant utilization to optimize a parameter of interest (e.g., the thrust-to-power ratio).

2) The screen and accelerator grid thicknesses (t_s and t_a, respectively) have also been treated as constants. For many beam cross-section geometries, it may be important instead to incorporate an equation into the analysis that relates the grid thicknesses required as a function of beam diameter or area. Such and equation could reflect the effects of discharge chamber power and the grid system mounting on thermally induced mechanical stresses in and deformation of the grids.

3) Although some variation in discharge chamber plasma properties has been incorporated into the development of the screen life constraint, there are other constraints that should also reflect the effects of plasma changes. For example, discharge voltage and propellant utilization influence the Maxwellian electron temperature and density and the primary electron energy and density. They in turn influence the baseline plasma ion energy cost and the doubly charged ion thrust factor. The effects of these changes on the thruster performance could be incorporated using currently available models.[20]

4) The grid spacing has been assumed constant across the entire intragrid region. The effects of variable spacing induced by thermal distortion and electric field-induced forces may cause the spacing to vary from one location to another. This would in turn influence the gross ion extraction and electrical breakdown characteristics of the grids.

Finally, it is noted that many of the parameters needed to model relevant plasma discharge and ion extraction phenomena can be computed from basic principles. A noteworthy exception is the primary electron containment factor ℓ^*. Approximate values can be inferred from experimental results,[11] but a model that can be used to calculate it for a discharge chamber with prescribed dimensions and magnetic field characteristics is needed. Additional work is also needed to describe more accurately the energy of primary electrons extracted from a hollow cathode as a function of discharge voltage and the sizes and potentials of the charge-exchange ion production regions within and downstream of the grids.

Conclusions

A methodology that can be used to determine the maximum power and thrust levels at which an ion thruster can be operated and a framework within which the resultant data can be presented has been developed. Physical constraints associated with allowable grid system span-to-gap ratio, intragrid electric field, discharge power per unit beam area, and screen and accelerator grid lifetimes have been identified as power and thrust limiting. Relationships that quantify each of these constraints have been developed. When the methodology is exercised for a thruster operating on xenon at propellant utilizations that effect maximum thrust-to-power operation and with constraints typical of existing thruster designs, results and trends that are generally consistent with experimental observations are obtained. Specifically, the span-to-gap constraint is found to be limiting at low specific impulses, and the intragrid electric field becomes limiting at higher ones. Increasing the allowable intragrid electric field from 2 to 4 kV/mm causes the limit on discharge power to become constraining at high specific impulses. Increasing the required screen and accelerator grid lifetimes from 10,000–20,000 h causes the accelerator grid lifetime to become limiting at intermediate specific impulses. Analysis also suggests the payload fraction delivered by a thruster operating at maximum thrust to power is relatively insensitive to specific impulse through a rather broad range around the optimum specific impulse.

Acknowledgments

Most of the background work described in this paper has been developed over a number of years under NASA Grant NGR-06-002-112. This financial support as well as the support of Vincent K. Rawlin and William R. Kerslake, who have given considerable technical guidance through that period, are gratefully acknowledged.

References

[1]Byers, D. C., and Rawlin, V. K., "Critical Elements of Electron Bombardment Propulsion for Large Space Systems," *Journal of Spacecraft and Rockets,* Vol. 14, No. 11, 1977, pp. 648–654.

[2]Byers, D. C., "Characterisistics of Primary Electric Propulsion Systems," AIAA Paper 79-2041, Oct. 1979.

[3]Kaufman, H. R., "Technology of Electron-Bombardment Ion Thrusters," *Advances in Electronics and Electron Physics,* Vol. 36, edited by L. Marton, Academic, New York, 1974, pp. 265–373.

[4]Rovang, D. C., "Ion Extraction Capabilities of Two-Grid Accelerator Systems," NASA CR-174621, Feb. 1984.

[5]Arakawa, Y., and Wilbur, P. J., "Discharge Plasma Calculations in Cusped Ion Thrusters Using the Finite Element Method," 20th AIAA/DGLR/JSASS International Electric Propulsion Conference, Paper 88-079, Oct., 1988.

[6]Langmuir, I., "The Interaction of Electron and Positive Ion Space Charges in Cathode Sheaths," *Physics Review,* Vol. 33, No. 6, 1929, p. 954.

[7]Feng, Y., and Wilbur, P. J., "Enhancement of Ion Beam Currents through Space-Charge Compensation," *Journal of Applied Physics,* Vol. 54, No. 11, 1983, pp. 6113–6118.

[8]Poeschel, R. L., and Beattie, J. R., "Primary Electric Propulsion Technology Study," NASA, Final Report on Contract NAS 3-21040, pp. 127–154.

[9]Kaufman, H. R., "Accelerator-System Solutions for Broad-Beam Ion Sources," *AIAA Journal,* Vol. 15, No. 7, 1977, pp. 1025–1034.

[10]Aston, G., and Wilbur, P. J., "Ion Extraction from a Plasma," *Journal of Applied Physics,* Vol. 52, No. 4, 1981, pp. 2614–2626.

[11]Brophy, J. R., "Ion Thruster Performance Model," NASA CR-174810, Dec. 1984.

[12]Bohm, D., "Mininmum Ionic Kinetic Energy for a Stable Sheath," *Characteristics of Electrical Discharges in Magnetic Fields,*

edited by A. Guthrie and R. K. Wakerling, McGraw-Hill, New York, 1949, pp. 77–89.

[13]Wilbur, P. J., and Kaufman, H. K., "Double Ion Production in Argon and Xenon Ion Thrusters," *Journal of Spacecraft and Rockets*, Vol. 16, No. 4, 1979, pp. 264–267.

[14]Beattie, J. R., Matossian, J. N., Poeschel, R. L., Rogers, W. P., and Martinelli, R., "Xenon Ion Propulsion Subsystem," AIAA Paper 85-2012, Sept.-Oct. 1985.

[15]Hyashi, M., "Determination of Electron-Xenon Total Excitation Cross Sections, from Threshold to 100 eV, from Experimental Values of Townsend's α," *Journal of Physics D: Applied Physics*, Vol. 16, No. 4, 1983, pp. 581–589.

[16]Rapp, D., and Englander-Golden, P., "Total Cross Sections for Ionization and Attachment in Gases by Electron Impact. I. Positive Ionization," *Journal of Chemical Physics*, Vol. 34, No. 5, 1965, pp. 1464–1479.

[17]Bohdansky, J., Roth, J., and Bay, H. L., "An Analytical Formula and Important Parameters for Low-Energy Ion Sputtering," *Journal of Applied Physics*, Vol. 51, No. 5, 1980, pp. 2861–2865.

[18]Rapp, D., and Francis, W. E., "Charge Exchange between Gaseous Ions and Atoms," *Journal of Chemical Physics*, Vol. 37, No. 11, pp. 2631–2645.

[19]Aston, G., and Kaufman, H. R. "Ion Beam Divergence Characteristics of Three-Grid Accelerator Sysems," *AIAA Journal*, Vol. 17, No. 1, 1979, pp. 64–70.

[20]Brophy, J. R., and Wilbur, P. J., "Calculation of Plasma Properties in Ion Sources," *AIAA Journal*, Vol. 24, No. 9, 1986, pp. 1516–1523.